Effects of porous covering on sound attenuation by periodic arrays of cylinders

Olga Umnova
School of Acoustics, Computer Science and Engineering
The University of Salford, Salford, Lancs. M5 4WT, UK

Keith Attenborough
Department of Engineering, University of Hull, Hull HU6 7RX, UK

Chris M. Linton
Department of Mathematical Sciences,
Loughborough University, Leics. LE11 3TU, UK

(porous covering effects in periodic arrays of cylinders)
Received:

PACS: 43.50 Gf, 43.20 Fn

Abstract

The acoustic transmission loss of a finite periodic array of long rigid cylinders, without and with porous absorbent covering, is studied both theoretically and in the laboratory. A multiple scattering model is extended to allow for the covering and its acoustical properties are described by a single parameter semi-empirical model. Data from laboratory measurements and numerical results are found to be in reasonable agreement. These data and predictions show that porous covering reduces the variation of transmission loss with frequency due to the stop/pass band structure observed with an array of rigid cylinders with similar overall radius and improves the overall attenuation in the higher frequency range. The predicted sensitivities to covering thickness and effective flow resistivity are explored. It is predicted that a random covered array also gives better attenuation than a random array of rigid cylinders with the same overall radius and volume fraction.

1. Introduction

Interest in applications of periodic arrays of cylinders for noise control has increased since publication of the measured transmission spectra of a minimalistic sculpture[1]. When the density of scattering elements is large enough, the structure does not support sound propagation through it at the frequencies of the stop-bands that appear in its transmission spectrum. Measurements on periodic arrays of cylinders[2] have shown the potential of using these kinds of structures for noise control. One possible advantage in using such periodic arrays instead of conventional noise barriers is that the structures are relatively transparent. Another possibility is that they could be formed from trees, since trees can be arranged in periodic arrays. Hence useful noise control could be achieved by natural means[3].

A 7.2m long, 11m wide periodic (triangular) array of hollow cylindrical PVC rods with diameter 16cm and with an array filling fraction, i.e. the volume fraction of cylinders in the array, of 47%, has been shown[2] to give a maximum attenuation close to 25dB at some frequencies in the range between 800Hz and 4kHz. However the transmission loss spectrum was found to have a peaky character and there were frequencies at which measured attenuation minima were less than 7dB. For noise control applications, the problem arises of how to reduce the frequency dependence of the attenuation without reducing the overall value. It has been suggested[2] that the effect of covering the elements by the sound absorptive materials should be investigated. This study is the main subject of the present paper.

Previous publications devoted to the study of the properties of sonic crystals refer to two theoretical approaches for predicting the transmission and reflection properties of the periodic arrays: the infinite array ‘sonic crystal’ approach, which involves the computation of the dispersion bands using a plane-wave expansion method[4,5] and the

multiple scattering approach[6,7]. The second approach is more useful for practical applications as it allows computations for finite arrays and direct comparisons with data**.**

Section 2 presents a review of the model used to describe multiple scattering by regular arrays and the modifications necessary to allow for porous coverings on the array elements. In Section 3, laboratory measurements on arrays of rigid and covered cylinders are described. Data for the insertion loss at different frequencies are compared with model predictions for the arrays of rigid and covered cylinders. Section 4 presents conclusions and suggestions for further research.

2. The model

In this paper we follow a previously-published multiple scattering approach[8]. However, we assume that a line source is located at the origin of the coordinate system instead of a source of plane wave excitation. Suppose that there are N cylinders of radius a_j^{out} and that the location of each cylinder center in the plane normal to the cylinder axes is described by one of N+1 polar coordinate systems in the (x,y) plane: (r,θ) centred at the origin and (r_j,θ_j), $j = 1,...,N$, centred at (x_j, y_j), the center of the j^{th} cylinder (Figure 1). The center-to-center spacing between the j^{th} and p^{th} cylinders is denoted by R_{jp} and the distance of the center of the j^{th} cylinder from the origin is denoted by S_j.

Exterior to the cylinders the pressure field is ϕ, where

$$\nabla^2\phi + k_0{}^2\phi = 0,$$

and $k_0 = \frac{\omega}{c_0}$ is the wave number in air.

Each cylinder scatters the waves which are incident upon it. To take account of all such scattering we express the total field as the sum of the incident wave $\phi_i = H_0(k_0 r)$ and a general outgoing wave emanating from each cylinder. Thus the total field exterior to the cylinders can be written

$$\phi = H_0(k_0 r) + \sum_{j=1}^{N} \sum_{n=-\infty}^{+\infty} A_n^j Z_n^j H_n^{(1)}(k_0 r_j) e^{in\theta_j}, \tag{1}$$

for some set of unknown coefficients A_n^j.

The factors Z_n^j are introduced for later convenience and determined by the boundary conditions on the cylinder surface.

If the cylinders are rigid

$$Z_n^j = \frac{J_n'(k_0 a_j^{out})}{H_n^{(1)\prime}(k_0 a_j^{out})}. \tag{2}$$

Using Graf's addition theorem for Bessel functions we can show that, as long as $r_p < R_{jp}$ for all $j \neq p$ and $r_p < S_p$, we can write:

$$\phi(r_p, \theta_p) = \sum_{m=-\infty}^{\infty} J_m(k_0 r_p) H_m^{(1)}(k_0 S_p) e^{im\theta_p} e^{-im(\pi+\sigma_p)} + \sum_{n=-\infty}^{\infty} A_n^p Z_n^p H_n^{(1)}(k_0 r_p) e^{in\theta_p}$$
$$+ \sum_{\substack{j=1 \\ \neq p}}^{N} \sum_{n=-\infty}^{\infty} A_n^j Z_n^j \sum_{m=-\infty}^{\infty} J_m(k_0 r_p) H_{n-m}^{(1)}(k_0 R_{jp}) e^{im\theta_p} e^{i(n-m)\alpha_{jp}}.$$

The geometrical restriction implies that this expression is only valid if the point (r_p, θ_p) is closer to the center of cylinder p than to the centers of any of the other cylinders or the source.

This is certainly true on the surface of cylinder p and so (2) can be used to apply the boundary conditions on each cylinder.

The cross section of the single element of the array with porous covering is shown in Figure 2. The field in the region $a_p^{in} < r_p < a_p^{out}$ can be represented by

$$\phi_{in}(r_p,\theta_p) = \sum_{n=-\infty}^{\infty} A_n^p \left(X_n^p H_n^{(1)}\left(k(\omega) r_p\right) + Y_n^p J_n\left(k(\omega) r_p\right)\right)$$

where $k(\omega)$ is complex wave number in the porous material and factors X_n^p and Y_n^p are again introduced for the later convenience.

We apply boundary conditions of continuity of pressure and particle velocity on the outer surface of the cylinder p:

$$\phi\Big|_{r_p=a_p^{out}} = \phi_{in}\Big|_{r_p=a_p^{out}}, \tag{3}$$

$$\frac{1}{\rho_0}\frac{\partial\phi}{\partial r_p}\Big|_{r_p=a_p^{out}} = \frac{\Omega}{\rho(\omega)}\frac{\partial\phi_{in}}{\partial r_p}\Big|_{r_p=a_p^{out}},$$

where $\rho(\omega)$ is complex density of porous material and Ω is its porosity.

At the interface between porous covering and the rigid core of the cylinder the condition of zero velocity is applied:

$$\frac{\partial\phi_{in}}{\partial r_p}\Big|_{r_p=a_p^{in}} = 0.$$

After using the orthogonality of the functions $e^{im\theta_p}$, $m = 0,\pm1,\pm2,\ldots$, these boundary conditions lead to an infinite system of equations for coefficients A_m^p.

$$A_m^p + \sum_{\substack{j=1 \\ \neq p}}^{N} \sum_{n=-\infty}^{\infty} A_n^j Z_n^j e^{i(n-m)\alpha_{jp}} H_{n-m}^{(1)}\left(k_0 R_{jp}\right) = -H_m^{(1)}\left(k_0 S_p\right) e^{-im(\pi+\sigma_p)}, \tag{4}$$

$$p = 1,\ldots,N, \qquad m = 0,\pm1,\pm2,\ldots.$$

which can be solved by truncation. These equations differ from those for rigid cylinders only by the factors Z_n^j which are determined from boundary conditions and are given by

$$Z_n^j = \frac{J_n\left(k_0 a_j^{out}\right) - Z(\omega) J_n'\left(k_0 a_j^{out}\right) F_n\left(k_0 a_j^{out}, k(\omega) a_j^{in}\right)}{H_n^{(1)}\left(k_0 a_j^{out}\right) - Z(\omega) H_n^{(1)}{}'\left(k_0 a_j^{out}\right) F_n\left(k_0 a_j^{out}, k(\omega) a_j^{in}\right)}, \tag{5}$$

where $F_n(x,y) = \dfrac{J_n(x) H_n^{(1)}{}'(y) - H_n^{(1)}(x) J_n'(y)}{J_n'(x) H_n^{(1)}{}'(y) - H_n^{(1)}{}'(x) J_n'(y)}$ and $Z(\omega) = \dfrac{\rho(\omega) k_0}{\Omega k(\omega) \rho_0}$ is the normalized characteristic impedance of porous material.

In principle, the model could be used for arrays of cylinders with different outer radii and different thickness of porous covering. However, since the measurements reported later have used arrays of identical cylinders, the simplified version of the model has been used for computations.

Equation (5) is expressed in terms of characteristic impedance $Z(\omega)$ and propagation constant $k(\omega)$, so, effectively, these quantities replace the porosity and the complex density function introduced by the boundary conditions (3). Although various models are available to provide $k(\omega)$ and $Z(\omega)$ as a function of frequency, since a fibrous woollen felt has been used in the measurements, the single parameter empirical Delany and Bazley model [9], derived from data for fibrous materials, has been found suitable. According to this model,

$$\begin{aligned} Z(\omega) &= 1 + 0.00571\left(\frac{\rho_0 \omega}{2\pi\sigma}\right)^{-0.754} + i0.087\left(\frac{\rho_0 \omega}{2\pi\sigma}\right)^{-0.732}, \\ k(\omega) &= \frac{\omega}{c_0}\left(1 + 0.0928\left(\frac{\rho_0 \omega}{2\pi\sigma}\right)^{-0.7} + i0.189\left(\frac{\rho_0 \omega}{2\pi\sigma}\right)^{-0.597}\right), \end{aligned} \tag{6}$$

where σ represents the flow resistivity of the material.

The numerical procedure for finding the total field at a certain point requires solving the system of equations (4) by truncation and finding the pressure by summation

using expression (1). For rigid cylinders, factors Z_n^j are determined from (2). If the cylinders are covered by porous material, the factors Z_n^j are determined from (5) and (6).

3. Measurements and comparisons of numerical results with data

Measurements have been carried out in a semi-anechoic chamber and far from any reflecting surfaces.

A free field ¼ inch B&K microphone was positioned centrally behind the array and orientated towards the source (Figure 3). The distance between the array and the microphone was varied between 3cm and 11.5 cm.

Sparks associated with air breakdown between high voltage electrodes have been used to provide acoustic pulses. The spark source was positioned 1.5 m away from the scattering array and 1m above the ground. The acoustic pulses had a duration of about 60μs and a central frequency of approximately15kHz (Figures 4a and 4b). Most of the acoustic energy of the pulse was contained between 1 kHz and 50 kHz. Outside this range the signal/noise ratio was too low for reliable results. Consequently the transmission loss measurements were limited to the range between 1 kHz and 50 kHz. Pressure measurements were made in the free field and then in the presence of the array. The spectral content of the signals was determined by Fourier transform. The insertion loss due to the array has been obtained from the ratio of the spectral density of the transmitted field in the presence of the array and that measured in the free field. The free field pressure data at various distances from the source are consistent with spherically spreading waves. However, since the model (equations (1) to (5)) is valid only for two dimensional geometry, the cylinders were sufficiently long (2 meters) that the receiver/ array distance (maximum 11.5 cm) was always much shorter than

the cylinder length. The rigid cylinders were aluminum rods with a diameter of 3/8 inch (0.953 cm) mounted between two rectangular supporting plates. Each absorbing cylinder had a ¼ inch (0.635cm)) diameter aluminum rod as a core and this was covered by a layer of woollen felt. The thickness of the felt was close to 1.7 cm so that the diameter of the covered cylinders (0.975cm) was close to that of the rigid cylinders used for the data comparison.

The cylinders were arranged in a square lattice, i.e. they were placed in identical rows so that the inter row distance was equal to the inter-cylinder distance within a row. This distance (2d) was chosen to be 1.5cm. The filling fraction of the rigid cylinder array was approximately 32% whereas the filling fraction of the corresponding square array of covered cylinders was 33%. Since the filling fractions of both arrays were more or less the same, any measured differences in their acoustical performance could be attributed exclusively to the presence of covering. The filling fraction of the rigid cylinder array was high enough for a stop/pass band structure to be noticeable in the attenuation spectrum. The arrays consisted of 3 rows with 7 cylinders in each row. This was the minimum number of rows needed for the stop/ pass bands to be observed when using rigid cylinders.

Figure 5 compares the measured insertion losses of the arrays of rigid and covered rods at 3 cm from the array. The presence of covering is seen to destroy the pass/stop band structure and to make the attenuation more uniform in frequency. In addition the sound absorbing nature of the porous covering provides stronger attenuation for most of the frequencies except in the first stop band. Between 10 kHz and 50kHz the minimum attenuation for the array of covered rods is 6.6 dB (at 10864Hz) and the mean value for the attenuation is 13.9dB. In the same frequency range the minimum

attenuation of the array of rigid cylinders is –2.2dB (at 17212Hz) and the mean attenuation is 6.9dB.

Figure 6 compares data and predictions for the array of rigid cylinders. To make similar comparisons for the array of covered cylinders the acoustical characteristics of the porous covering material are required. Surface impedance values have been deduced from measurements of the complex excess attenuation, i.e. the ratio between the pressures measured by the receiver arranged above the felt layer and in the free field [10]. The complex excess attenuation is related to the spherical wave reflection coefficient Q by

$$EA = 1 + Q\frac{R_1}{R_2}e^{ik_0(R_2 - R_1)},$$

where R_1 and R_2 are the direct path length from the source to receiver and the path length through the specular reflection point respectively**.** The relationship between the spherical wave reflection coefficient Q and the surface impedance Z of the porous layer is obtained from:

$$Q = R(1 - F(w)) + F(w),$$
$$R = \frac{1 - Z_s\cos(\Theta)}{1 + Z_s\cos(\Theta)}$$
$$F(w) = 1 + i\sqrt{\pi}we^{-w^2}erfc(-iw),$$
$$w = \sqrt{\frac{ik_0R_2}{2}}\frac{1 + Z_s\cos(\Theta)}{Z}.$$

Hence the surface impedance Z_s can be deduced from the excess attenuation data using a numerical method to search for complex roots.

The surface impedance of the hard-backed porous layer is related to the propagation constant $k(\omega)$ and the characteristic impedance of the material $Z(\omega)$:

$$Z_s = \frac{Z(\omega)}{\cos(\Theta_T)}\coth(-ik(\omega)d\cos(\Theta_T)),$$
$$\Theta_T = \sin^{-1}\left(\sin(\Theta)\frac{k_0}{k(\omega)}\right). \quad (7)$$

Using (6) and (7) and a least squares method, the value of the flow resistivity parameter σ in the Delany and Bazley model has been adjusted to fit the surface impedance data for both single and double layers of felt. Figure 7 shows the surface impedance data and the best-fit predictions. It appears that the Delany and Bazley model (6) with σ=23 kPa s m^{-2} provides a good approximation to the characteristic impedance and the propagation constant in the frequency range of interest. The results presented here are limited by the extent to which the Delany and Bazley model is applicable. For example, other work [11] has shown that this model overestimates the attenuation constant within a rigid-porous material for a given flow resistivity. Moreover, since the felt used for the covering does not correspond to the type of fibrous material (e.e. glass fiber) for which the Delany and Bazley model was intended, the best fit flow resistivity represents an *effective* value**.**

Comparisons between predictions and data for the insertion loss of the array of covered cylinders are shown in Figure 8 for the microphone was positioned either 3 cm from the array or 11.5 cm from the array. This change in distance from the array does not appear to affect the attenuation significantly. The mean attenuation between 10 kHz and 50kHz is 14.0dB with the receiver 11.5 cm from the array. This is very close to that (13.9 dB) observed with the receiver 3cm from the array.

The sensitivity of the results to the thickness of the porous covering has been studied numerically by performing computations for various covering thickness while keeping the outer radius of the cylinder constant, thus keeping the filling fraction of the array constant. According to the predictions in Figure 9, increase in the covering

thickness does not necessarily mean improved attenuation. A covering thickness increased to 5/2 of its original value (0.438 cm), corresponding to nearly all of the cylinders consisting of porous material, does not show the best performance in any frequency range. This suggests that there is an optimum thickness for a given flow resistivity.

Figure 10 shows predictions for σ = 11.5, 23 and 69 kPa s m^{-2}. The largest mean attenuation corresponds to the highest flow resistivity value. On the other hand, when the flow resistivity and hence the surface impedance of the covering are sufficiently high the results should be comparable with those for acoustically-hard cylinders. Indeed, for the given array, it has been found that the hard cylinders prediction is recovered when σ=10^4 kPa s m^{-2}. However the Delany and Bazley model is only applicable when $10^{-2} < \frac{\omega}{2\pi\sigma} < 1$ ($\frac{\omega}{2\pi\sigma}$ measured in SI units). This means that, strictly speaking, the model can only be applied for frequencies higher than 100kHz which is well outside the measured range. Consequently a more sophisticated model for the acoustical properties of the porous covering would be needed to find the optimum flow resistivity value.

To predict the effect of randomizing the array, each cylinder centre has been moved at random from its location in regular array (x_j, y_j) [12]. Hence the coordinates of each cylinder in the perturbed array are:

$$x'_j = x_j + \tau\gamma_j\left(d - a^{out}\right)\cos(2\pi\beta_j),$$
$$y'_j = y_j + \tau\gamma_j\left(d - a^{out}\right)\sin(2\pi\beta_j),$$

where γ_j and β_j are random numbers from the interval [0,1] and parameter τ determines the proportion of the maximum permissible displacement $(d - a^{out})$ of the cylinders. In the computations it was assumed that $\tau = 0.9$ so that the imposed

order of disorder was relatively high. Since different results are obtained for each 'random' array, computations of the transmitted field have been carried out for 10 arrays and the results have been averaged. Figure 11 shows that a random array of cylinders covered by single layer of felt is predicted to provide better attenuation than a similarly random array of hard cylinders. The difference in averaged attenuation is approximately 4.5dB.

4. Conclusions

Laboratory measurements and numerical simulations of the transmission loss of regular cylinder arrays, using a multiple scattering model modified to allow for the porous r covering, have shown that covering the cylinders with a porous material makes the array insertion loss more uniform in frequency. Moreover arrays with covered elements provide higher averaged attenuation than similar arrays of rigid cylinders. Numerical simulations have shown that the insertion loss depends strongly on the covering thickness and that a thicker porous covering does not necessarily means better attenuation. On the other hand increasing the flow resistivity of the covering material by a factor of three is predicted to improve the array performance. These results suggest that it might be possible to optimize the array attenuation through choice of covering material and its thickness. It might be worthwhile to explore the use of multiple layers for impedance matching in the porous covering also.

In the laboratory measurements considerable attenuation has been achieved in the frequency range between 10kHz and 50kHz by the array with a filling fraction of 33%. To achieve a similar attenuation in noise control applications that would involve a lower frequency range, the geometry of the cylinder arrays would have to be scaled

accordingly. If it is supposed that lowering the frequencies by a certain factor will mean that the distances should be increased by the same factor, to offer a useful attenuation in the frequency range between 300Hz and 1.5kHz the distance between cylinders and rows should be approximately 45 cm and the cylinders diameter would have to be approximately 30cm. In an artificial array intended for outdoor use the choice of porous material would be limited by the ability to withstand weathering and fibrous materials may not be suitable. Consequently simulations and measurements using more robust materials such as porous concrete are needed. The potential for use of periodic arrays of trees has been demonstrated already [3] but there may be possibilities for exploiting species with high porosity and/or roughness of bark. Finally, the performance of arrays in which trees are surrounded by foliage might be simulated through a covered cylinder model of the kind presented here.

Acknowledgement

We are grateful to Dr. Q. Qin, University of Hull, for the complex excess attenuation measurements and deduction of the felt impedance.

The work was supported by EPSRC Grant GR/S35592 while the first author was at the University of Hull.

References

[1]R. Martinez-Sala, J. Sancho, J. V. Sanchez, V. Gomez, J. Llinares, and F. Meseguer, "Sound attenuation by sculpture", Nature, 378, 241, (1995)

[2]J.V.Sanchez – Perez, C. Rubio, R.Martinez-Sala, R.Sanchez-Grandia, V.Gomez "Acoustic barriers based on periodic arrays of scatterers", Appl.Phys.Lett., 81, 5240-5242, (2002)

[3]R.Martinez-Sala, C.Rubio, L.M.Garcia-Raffi, J.V.Sanchez-Perez, E.A.Sanchez-Perez, J.Llinares "Control of noise by trees arranged like sonic crystals", to be published in Journal of Sound and Vibration

[4]J.V.Sanchez-Perez, D.Caballero, R.Martinez-Sala, C.Rubio, J.Sanchez-Dehesa, F.Meseguer, J.Llinarez, F.Galvez, "Sound attenuation by a two-dimensional array of rigid cylinders", Phys.Rev.Lett., 80, 5325-5328 (1998).

[5]D.Caballero, J.Sanchez-Dehesa, C.Rubio, R.Martinez-Sala, J.V.Sanchez-Perez, F.Messeguer, J.Llinares, "Large two-dimensional sonic band gaps", Phys.Rev.E, 60, R6316-R6319, 1999.

[6]Y.-Y.Chen, Z.Ye "Theoretical analysis of acoustic stop bands in two-dimensional periodic scattering arrays", Phys.Rev.E, 64, 036616, (2001)

[7]Y.-Y.Chen, Z.Ye, "Acoustic attenuation by two-dimensional arrays of rigid cylinders", Phys.Rev.Lett. 87, 184301, (2001)

[8]C.M.Linton, D.V.Evans, "The interaction of waves with arrays of vertical cylinders", J. Fluid Mech. 215, 549-569, (1990)

[9]M.E.Delany, E.N.Bazley "Acoustic properties of fibrous absorbent materials", Applied Acoust., 3, 105-116, (1970).

[10]P. Boulanger, K. Attenborough, Q. Qin "Effective impedance of surfaces with porous roughness: Models and data", J.Acoust.Soc.Am., 117, 11146-156, (2005)

[11]J-F Allard, Sound propagation in porous media, Elsevier Applied Science 1993

[12]G.Duclos, A.H.Clement "Wave propagation through arrays of unevenly spaced vertical piles", Ocean Engineering 31, 1655-1668, (2004).

Figure captions.

Figure 1. Plan view of two cylinders and corresponding Cartesian and polar coordinates

Figure 2. Cross section of the cylinder covered with porous material.

Figure 3. Measurement arrangement and geometry

Figure 4. Waveform (A) and spectrum (B) of the pulse generated by the spark source, distance from the source 150cm.

Figure 5. Effect of the porous covering on the attenuation spectrum at 3cm from the regular array. The solid line represents data for rigid cylinders; the broken lines represents data for rigid cylinders covered with felt.

Figure 6. Measurements (solid line) and model predictions for the insertion loss of the array of rigid cylinders for a receiver 3cm from the array.

Figure 7. Surface impedance of single (a) and double (b) layer of felt. Points – data, lines – predictions, using Delany and Bazley model for characteristic impedance and propagation constant with $\sigma = 2.3 \times 10^4 \, Pa\, s / m^2$.

Figure 8. Data (points) and predictions (broken lines) for the attenuation spectrum of the array of covered rods (a) at a receiver 3 cm from the array, (b) at a receiver 11.5 cm from the array.

Figure 9. Predicted insertion losses at 3cm from the array for 33% filling fraction regular arrays with different felt covering thickness. The dotted line represents predictions with 0.088cm covering thickness; the solid line represents predictions with 0.175cm covering thickness; the broken line represents predictions with 0.35cm covering thickness; the dashed dotted line represents predictions with 0.438cm covering thickness.

Figure 10. Predicted insertion losses at 3 cm from arrays of cylinders covered by different flow resistivity materials. All dimensions are as in Figure 6. The solid line - $\sigma = 23000$ Pa s/m^2 (felt), dashed dotted line - $\sigma = 11500$ Pa s/m^2, dashed line - $\sigma = 69000$ Pa s/m^2.

Figure 11. Predicted insertion loss of an array with randomised positioning of the cylinders, 3cm from the array. Array dimensions as for Figure 6. The solid line represents predictions for an array of rigid cylinders. The broken line represents an array of cylinders covered with felt.

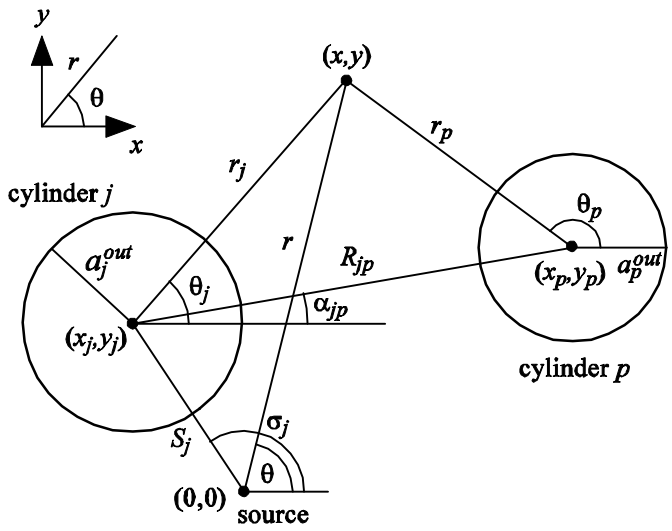
y
r
θ
x
(x,y)
r_j
r_p
cylinder j
θ_p
r
R_{jp}
a_j^{out}
θ_j
(x_p,y_p)
a_p^{out}
α_{jp}
(x_j,y_j)
cylinder p
σ_j
S_j
θ
(0,0)
source

Figure 1

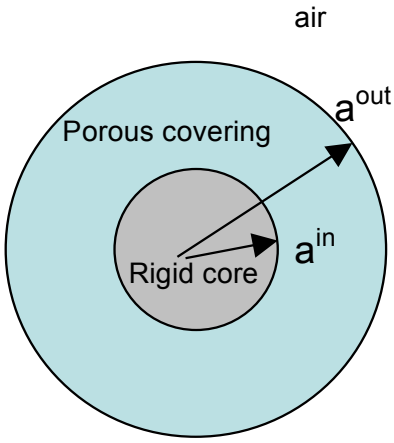

Figure 2.

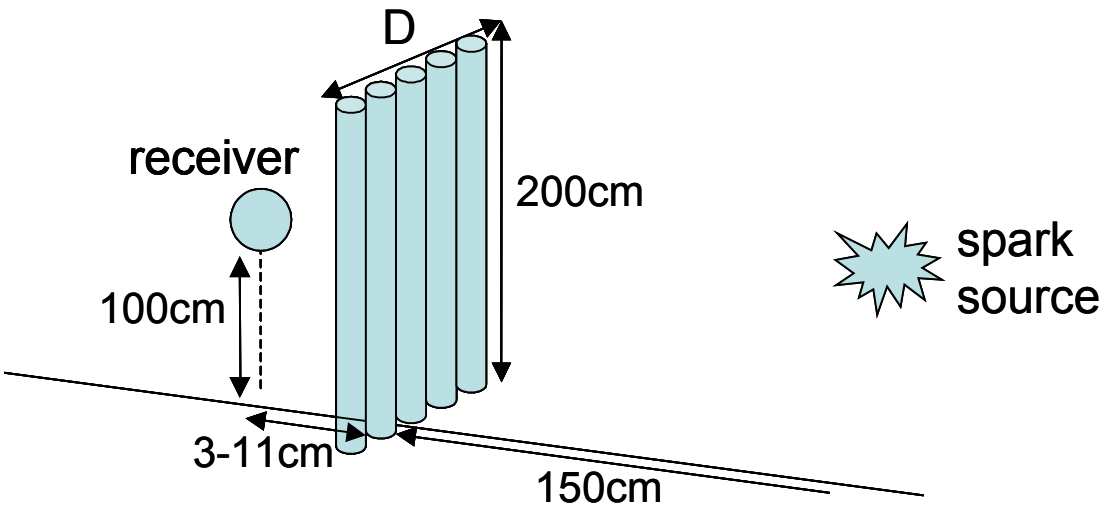

Figure 3.

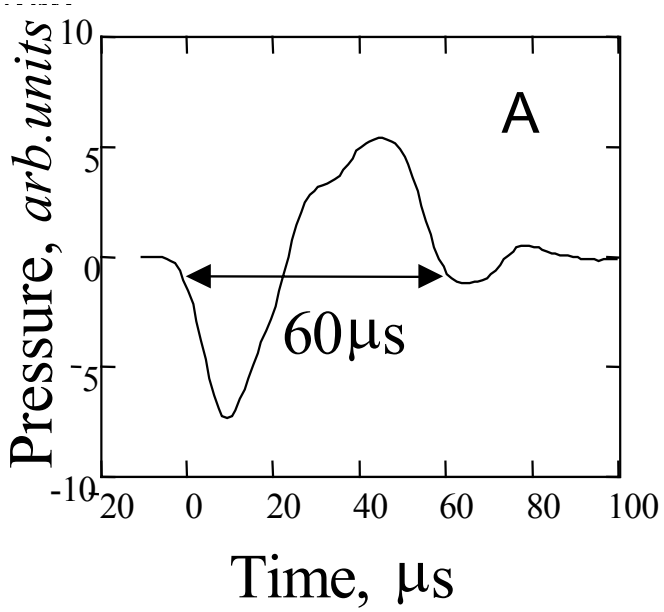
Pressure, arb.units
10
5
0
-5
-10
A
60μs
-20
0
20
40
60
80
100
Time, μs

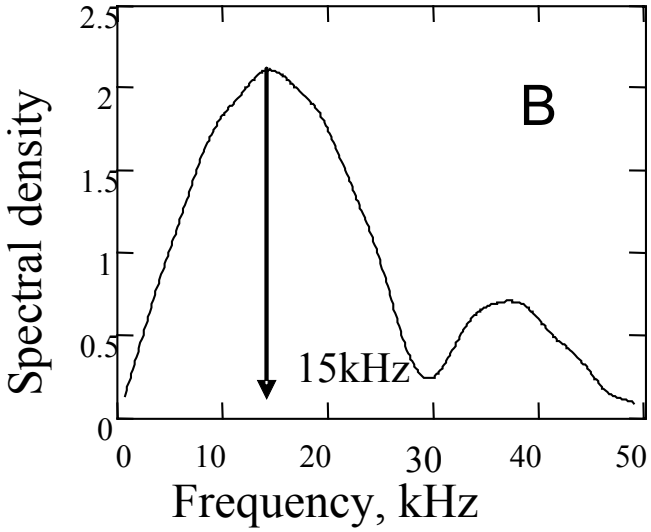
Spectral density
2.5
2
1.5
1
0.5
0
B
15kHz
0
10
20
30
40
50
Frequency, kHz

Figure 4.

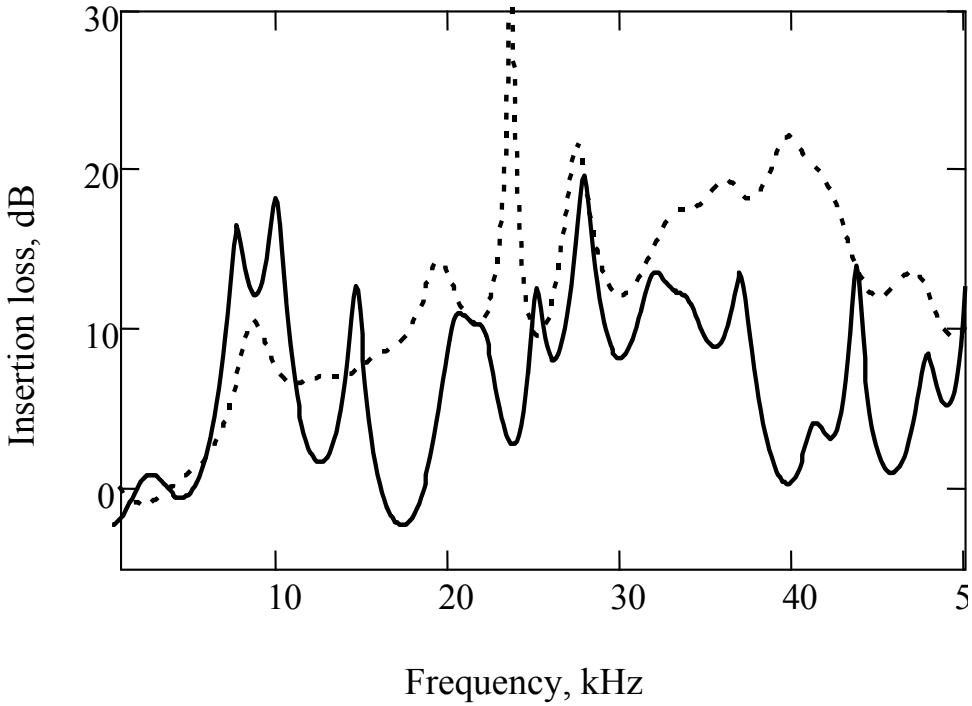

Figure 5.

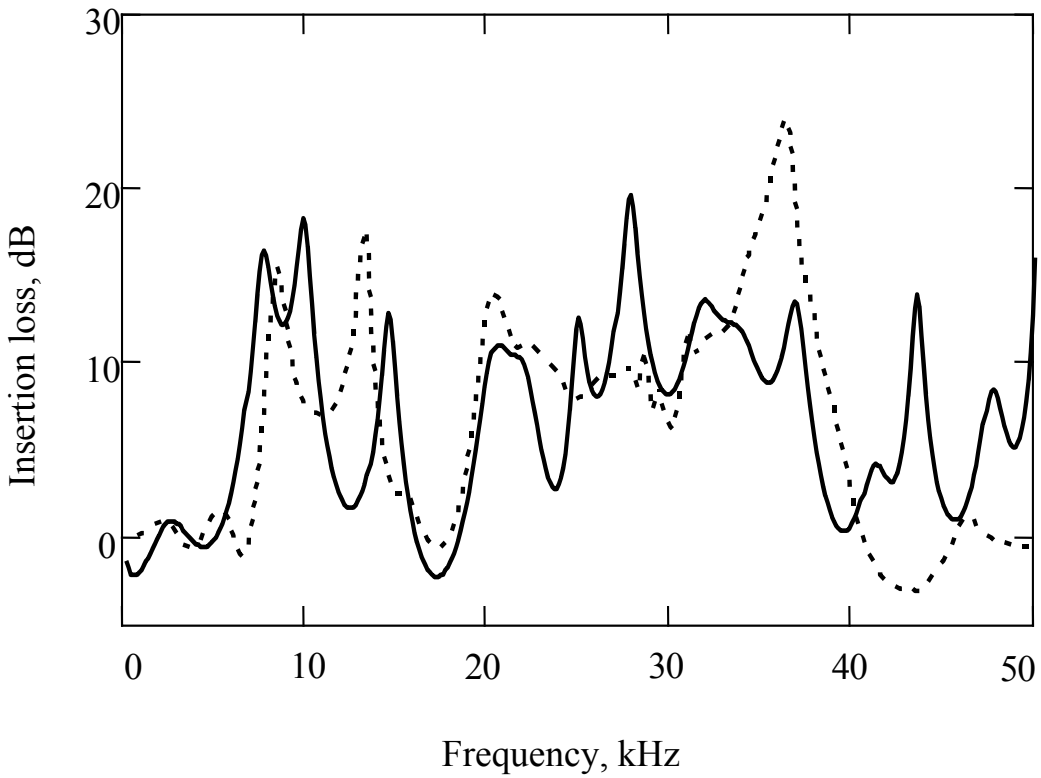

Figure 6.

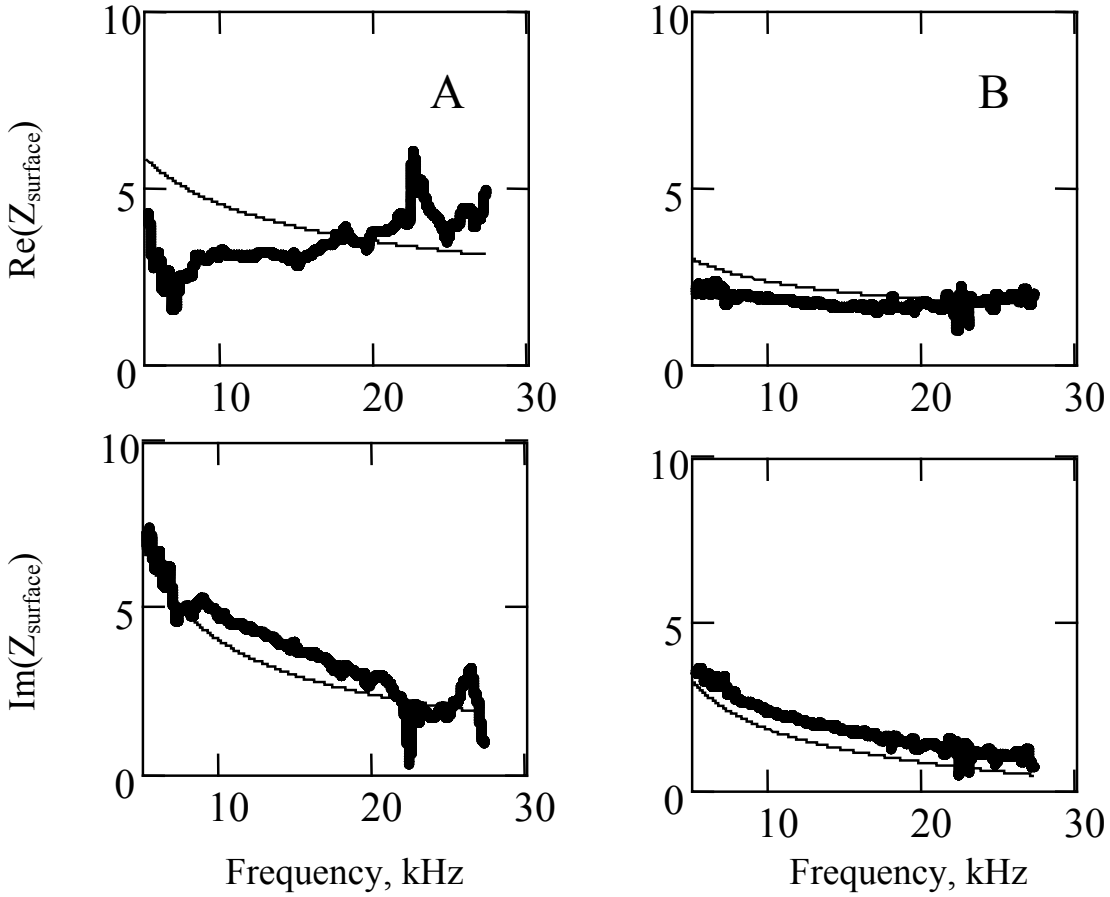

Figure 7.

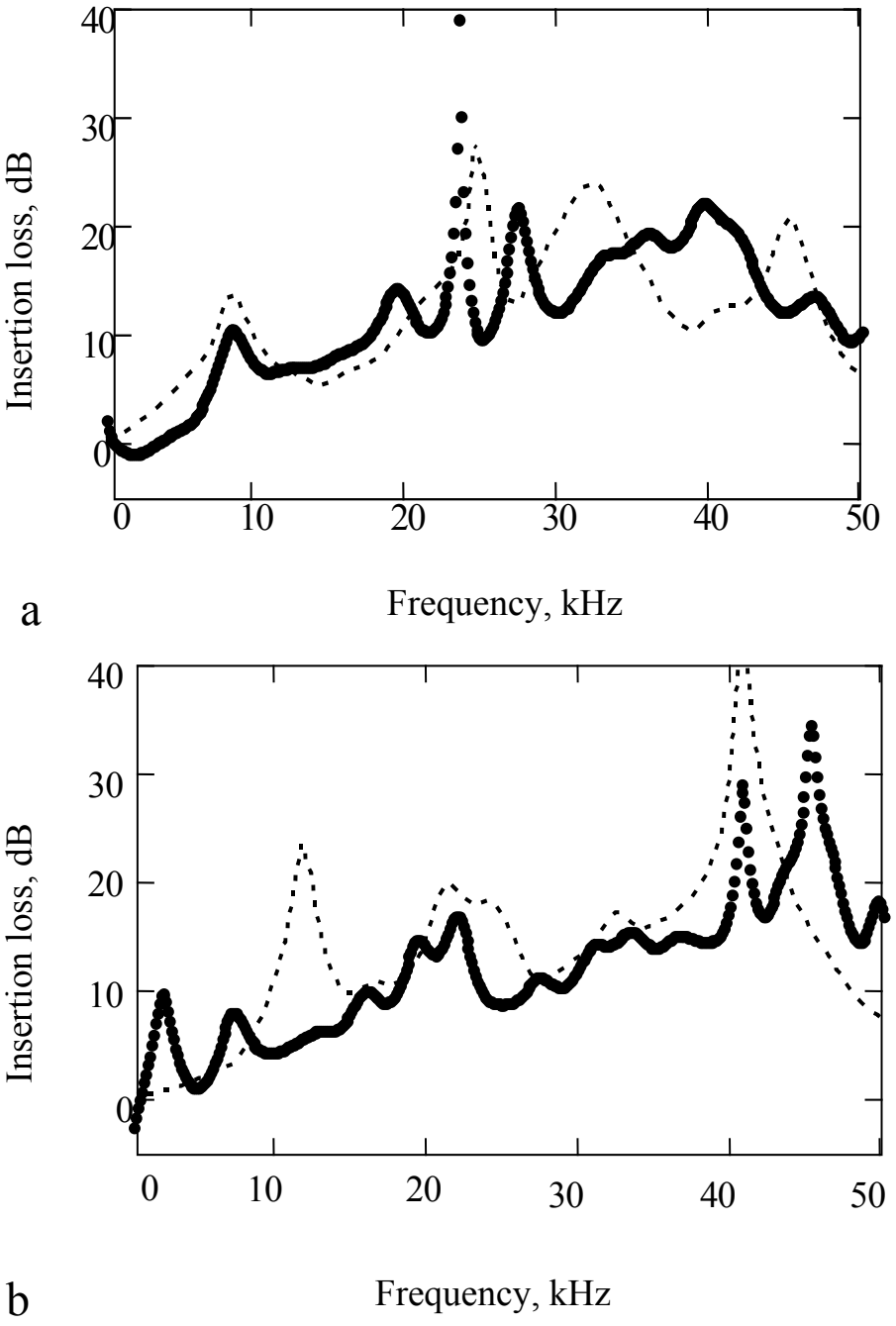
40
30
20
10
0
Insertion loss, dB
0
10
20
30
40
50
Frequency, kHz
a
40
30
20
10
0
Insertion loss, dB
0
10
20
30
40
50
Frequency, kHz
b

Figure 8.

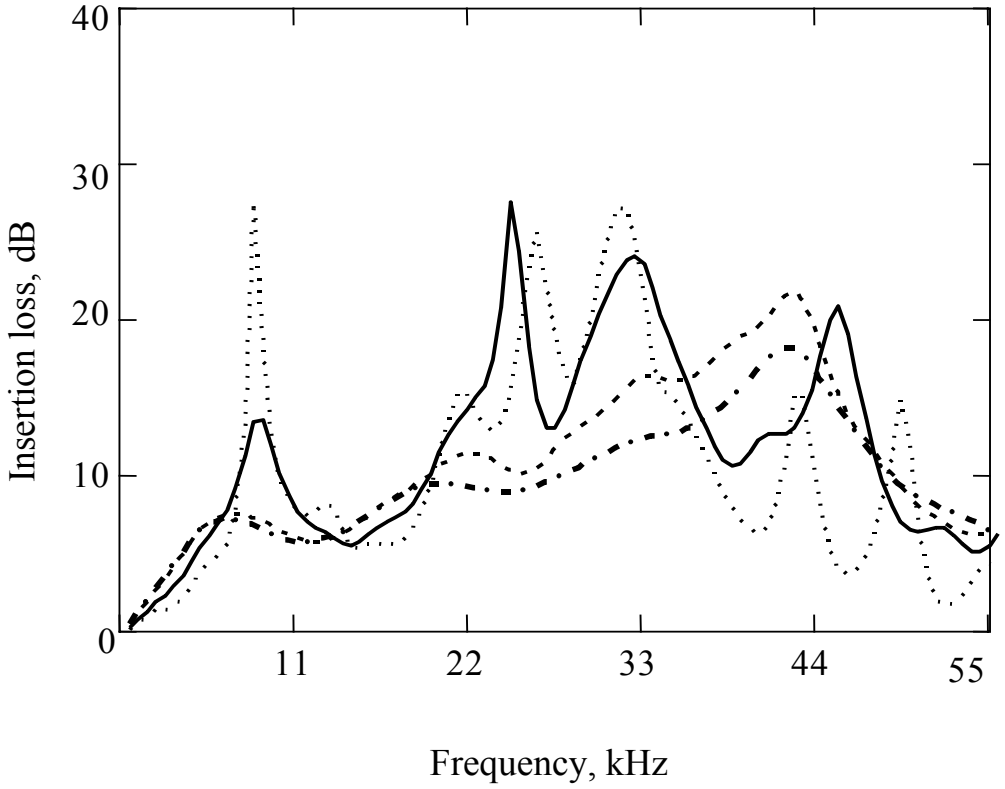

Figure 9.

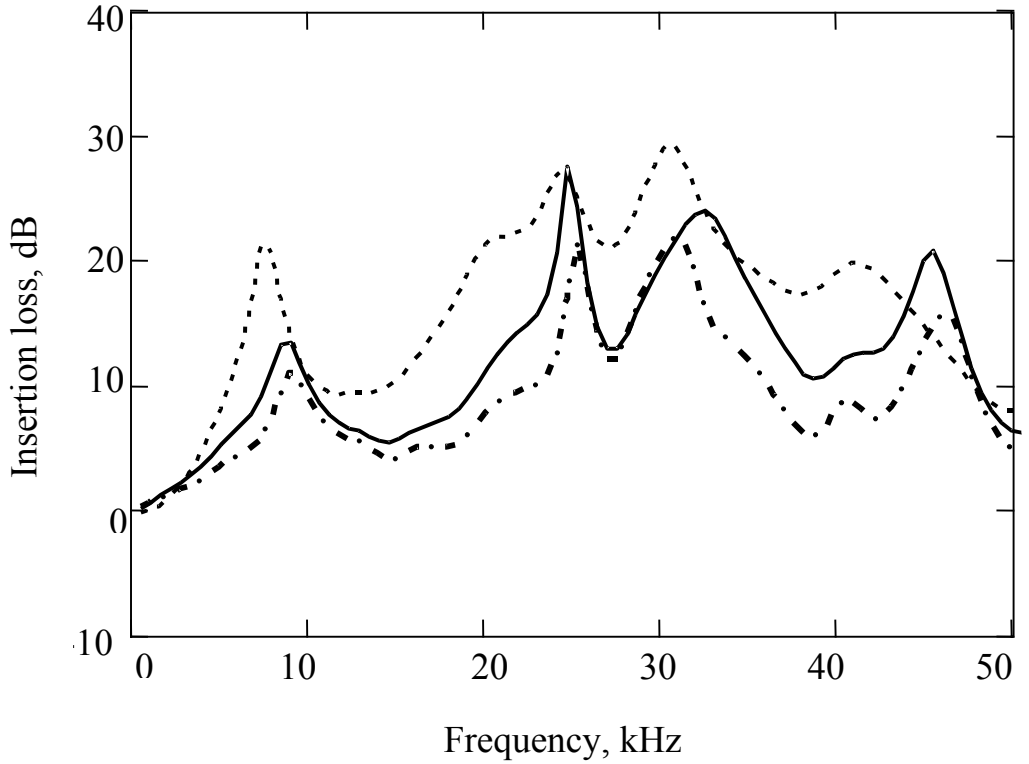

Figure 10.

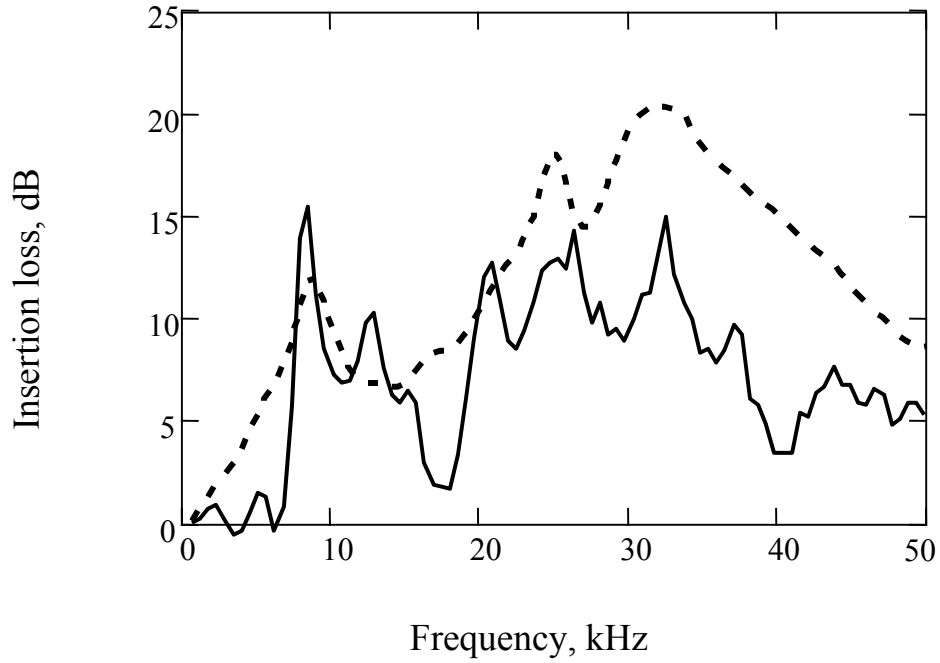

Figure 11.